Estimation of tidal energy potential in the Vietnam East Sea: A comprehensive analysis using semi-empirical tide models

Loc Nguyen-Xuan [a,*], Tuan Nguyen-Le [b], Quan Tran-Anh [c], Long Trinh-Tuan [d]

[a] Center for Environmental Fluid Dynamics, VNU University of Science (VNU-HUS), Viet Nam
[b] Vietnam Environment and Marine Sciences Institute (VEMSI), Viet Nam
[c] Faculty of Environment, Hanoi University of Mining and Geology (HUMG), Viet Nam
[d] Vietnam Academy for Water Resources (VAWR), Viet Nam

ABSTRACT

This study assesses the tidal energy potential in the Vietnam East Sea (VES), a region with complex hydrodynamics and significant interactions with the Western Pacific Ocean. A rigorous validation of six prominent semi-empirical global ocean tide models (FES2014, DTU16, EOT20, GOT4.10c, HAMTIDE12, OSU12.V1) was conducted against an extensive network of 34 tide gauge stations in the VES region. The validation identified FES2014 as the superior model, exhibiting the closest agreement with observations due to its advanced data assimilation techniques, high-resolution grids, and robust hydrodynamic representation influenced by the complex VES bathymetry. Leveraging the FES2014 model, the influential role of the semi-diurnal component (M_2) in dictating energy distribution is prominently evident. Evaluation results of tidal amplitudes revealed three emerging hotspots: the Batang Lupar estuary (Malaysia), Anpu Gang (China), and Bac Lieu (Vietnam), with tidal amplitudes up to 326.2 cm. The Anpu Gang exhibited the highest theoretical potential tidal energy of 14.90 Wh/ m^2, making it the most promising site for localized tidal power development. Although moderate compared to globally renowned sites, the identified VES hotspots merit consideration for small-to-medium scale projects tailored to local conditions. While limited to potential energy assessments, this study provides a crucial baseline for the VES region, highlighting opportunities for sustainable tidal energy exploitation.

1. Introduction

The global energy crisis has emerged as one of the most pressing issues facing nations worldwide in recent years. According to the Wiatros-Motyka et al. (2023), there was a staggering 694 TWh increase in worldwide electricity consumption in 2022. This surge in demand placed immense strain on major markets, leading to unprecedented price levels and a record-breaking spike in emissions from the power sector. Electricity has become an indispensable part of modern life, and the transition to clean, renewable energy sources is more crucial than ever before. Among the various renewable energy alternatives to fossil fuels and nuclear power, tidal energy has garnered significant attention from the scientific and engineering communities. Using tidal energy is a promising solution for electricity generation while mitigating the substantial environmental pollution associated with traditional energy sources. The total tidal energy is derived from the sum of potential and kinetic energy components (Gorlov, 2009). Understanding the potential energy of tides is crucial for designing tidal power plants that utilize dam structures to generate water columns, harnessing the energy by raising and lowering water vertically. On the other hand, the kinetic energy of tides is harnessed in floating tidal power plants or other systems that capture the energy from tidal currents or horizontal flow. These types of plants do not require the construction of dams. Currently, there are three primary methods for generating tidal energy including tidal barrages, tidal lagoons, and tidal streams (Shetty and Priyam, 2022). Tidal currents are the most common phenomena observed in the coastal ocean and estuaries (Amedo-Repollo et al., 2021). Several global studies have indicated that marine current energy (kinetic energy) holds significant potential as a clean, predictable, and environmentally friendly source for electricity production compared to tidal barrages (Dai et al., 2018; Domenech et al., 2018). As a result, current research efforts in tidal energy have primarily focused on kinetic energy and associated extraction technologies, with less emphasis on evaluating potential energy.

---

* Corresponding author.
  E-mail address: nxloc@hus.edu.vn (L. Nguyen-Xuan).

Covering 70 % of the Earth's surface, the ocean represents a vast source of renewable energy that, if harnessed properly, could help meet the growing global energy demand (Abd Rahim et al., 2023). The ocean contains more than 2×10^3 terawatts of renewable energy, encompassing thermal energy, wave and tidal energy, and the energy at the interface where rivers meet the ocean (Mao et al., 2024). Unlike other renewable sources like wind, solar, and geothermal, tidal energy possesses the unique advantage of being predictable in timing and magnitude for centuries ahead. Variations in tidal height on semidiurnal, diurnal, semimonthly, monthly, semiannual, and longer scales are attributed to the combined movements of the Moon around Earth and Earth around the Sun (Kvale, 2006). These cyclic movements allow for accurate long-term predictions of tidal patterns. However, harnessing this energy source presents challenges due to its wide distribution across expansive areas. Nevertheless, with its high predictability, high energy density, and significant potential for electricity generation, tidal energy's prospects for development are very promising (Shao et al., 2023).

Tidal energy development has gained momentum recently, although progress has been relatively slow. Several tidal energy power plants are currently operational worldwide (Table 1), indicating the growing interest in this renewable energy source. Among these plants, the Sihwa Tidal Power Station in South Korea stands as the largest, boasting a capacity of 254 MW (Bae et al., 2010). France is also prominently in the tidal energy landscape, hosting major power plants such as the Rance Tidal Power Station (Charlier, 2007). In Canada, the Annapolis Royal Tidal Station (Waters and Aggidis, 2016) contributes to global efforts in harnessing tidal energy. In addition, some other tidal power plants include Kislaya Guba (Russia) (Bernshtein, 1972), Jiangxia (China) (Wang and Wang, 2019), Eastern Scheldt Barrier (Netherland) (Bui, 2010), Bluemull (UK) (Neill et al., 2017) and Pempa'q In-stream (Canada) (Li, 2021).

The Vietnam East Sea (VES), also known as the South China Sea, presents a promising opportunity for tidal energy generation due to its vast expanse and relatively shallow nature. According to the International Renewable Energy Agency, the VES has the potential to generate up to 8.2 gigawatts of tidal energy (Zheng et al., 2015). That is equivalent to the electricity needs of over 2 million homes. However, despite its potential, limited research has been conducted on tidal energy in this region.

Early investigations into tidal patterns in the VES revealed a wide range of descriptions for tidal characteristics in the continental shelf regions. Researchers such as Sergeev (1964) produced co-tidal charts based on various datasets, highlighting the diversity of tidal behaviour. Since the 1980s, different methods have been employed in tidal studies of the VES. These approaches include analyzing tidal harmonic constituents using data from 320 observation stations. Additionally, researchers like Yanagi et al. (1997) and Jian-yu et al. (2001) utilized Topex/Poseidon (T/P) altimetry data, while Ye and Robinson (1983)

employed numerical models. These previous modeling studies focused on solving the two-dimensional (2D) depth-integrated shallow water equations and utilized open boundary conditions for elevation derived from limited local tidal observations or interpolated from historical co-tidal charts. In the past few years, the continuously advancing and enhancing field of ocean tide modeling has led to substantial improvements in the precision of predicting ocean tides (Shum et al., 1997; Stammer et al., 2014).

One type of ocean tide model, known as semi-empirical, is derived from empirical harmonic analysis of satellite altimetry data relative to a reference model. These semi-empirical tide models rely heavily upon satellite altimetry data. Recently, significant advancements have been made to coastal altimetry in several fields, including critical improvements in correction fields, more detailed and coastal-specific data editing, and new schemes for radar echo analysis (retracking). Piccioni et al. (2018) demonstrated an improvement more significant than two cm for single tidal constituents when using the ALES (Adaptive Leading Edge Sub Waveform, Passaro et al., 2014) retracker that enhances the performances of sea level retrieval in the coastal region and the corresponding correction for sea state bias (Passaro et al., 2018). The continued developments of altimetry in the coastal region and the increased number of altimetry missions have positively impacted the models' ability to estimate ocean tides accurately.

Several models within this category are presently commonly employed, including EOT, FES, DTU, GOT, HAMTIDE, and OSU. These models have undergone extensive scrutiny across numerous global monitoring stations, validating their high degree of accuracy. However, their applicability to the VES region must be more investigated with validation against a comprehensive network of monitoring stations. Assessing the suitability of various semi-empirical models will determine which models can be employed to study potential energy. Several studies, such as Neill et al. (2021) on the tidal range resource of Australia, use semi-empirical models to investigate tidal energy. However, evaluating tidal potential energy within the VES using data from semi-empirical models has been notably lacking. Existing studies on tidal energy have primarily focused on utilizing Tide Tables, as seen in Yusoff et al. (2015), or at specific measurement points, as illustrated by Nazri et al. (2018), without delving into the exploration of tidal energy, particularly in terms of potential energy, across the entire VES. Using data derived from semi-empirical tide models presents an avenue for exploring novel research trajectories and applications within the domain of tidal energy analysis specific to the VES. Thus, the primary objective of this study is to comprehensively assess and validate the performance of widely recognized semi-empirical tide models using extensive datasets. The studies analyze the data to determine tidal energy generation's viability at various VES locations. The findings of this research are expected to provide valuable insights and guidance for tidal studies and the future development of tidal energy projects in the region, contributing to the sustainable energy transition in the VES area.

2. Data and methods

2.1. Study area

The VES is a region characterized by various environments, including deep sea areas, coastal shallows, and reef islands (Sun et al., 2020). It is shared among several countries: China, Vietnam, Philippines, Malaysia, Brunei, Thailand, Indonesia, and Cambodia. The VES, situated between 99 and 122°E and 0–25°N along the Eurasian plate's edge, comprises a deep basin and two continental shelves (around 55 % of its total size) along the north and southwest coasts. Within the northern VES region, a linkage between the VES and the East China Sea is established via the Taiwan Strait. Additionally, the VES is accessible to the Pacific Ocean through the Luzon Strait. The basin's southern part is connected to the Java Sea through the Karimata Strait and to the Sulu Sea through narrow channels between the Philippine

Table 1
Operational tidal power plants.

Power plant	Country	Year Commissioned	Avg. tide (m)	Capacity (MW)
La Rance	France	1966	8.2	240
Kislaya Guba	Russia	1968	2.3	1.7
Jiangxia	China	1980	5.1	3.9
Annapolis	Canada	1984	6.4	20
Uldolmok	South Korea	2009	3.0	1.0
Sihwa Lake	South Korea	2011	5.6	254
Eastern Scheldt Barrier	The Netherlands	2015	2.5	1.2
Bluemull Sound	United Kingdom	2016	1.58	0.5
MeyGen14	United Kingdom	2017	2.26	6.0
Pempa'q In-stream	Canada	2022	16.0	9.0

Islands (Fig. 1).

The VES is a highly dynamic marine environment, where complex interactions between various physical processes shape the tidal and wave energy regimes. The intricate bathymetry of the VES, with its deep basin, continental shelves, and numerous islands and reefs, significantly influences the distribution and dissipation of tidal energy (Zu et al., 2008; Morozov, 1995). The tidal dynamics in the VES are primarily dominated by the semi-diurnal (M_2) and diurnal (K_1) constituents, which interact with the complex seafloor topography to produce complex patterns of tidal energy distribution (Morozov, 1995; Egbert and Ray, 2000; Niwa and Hibiya, 2004). Studies have shown that the steep continental slopes and underwater ridges in the VES act as barriers, leading to the scattering and dissipation of surface tides (Rainville and Pinkel, 2006). This scattering process generates internal tides, which can propagate over long distances and interact with the background circulation (Gan et al., 2006; Zu et al., 2008).

The bathymetric features of the VES also play a crucial role in the generation and propagation of internal waves. The sharp changes in seafloor depth, particularly over seamounts and ridges, can lead to the generation of high-amplitude internal waves through the interaction of tidal currents with the seabed (Rainville and Pinkel, 2006). These internal waves can transport significant amounts of energy and influence the mixing and circulation patterns in the region (Yang et al., 2014). Moreover, the amplitudes of tides on the continental shelf or in semi-enclosed embayments can become more amplified due to

resonance phenomena within a reflective system (Feng et al., 2021).

While the Vietnam East Sea (VES) experiences pronounced seasonal variations in circulation patterns driven by the East Asian monsoon system, these seasonal changes have limited direct impact on tidal range and amplitude. The fundamental astronomical forces governing tides remain constant throughout the year, maintaining the primary tidal constituents (M_2, S_2, K_1, P_1, O_1) relatively stable (Huang et al., 2022). However, seasonal shifts in circulation, such as the alternation between northward and southward flows in the southern VES (Chen et al., 2012; Shuai et al., 2021), primarily affect background conditions rather than tidal amplitudes themselves. While interactions between internal tides and barotropic tides can cause variations in tidal phases (Li et al., 2020; Xie et al., 2018), these do not typically result in significant changes to overall tidal amplitudes. Thus, while the VES exhibits a dynamic oceanographic environment with various seasonal phenomena (Hu et al., 2020; Zhou and Wang, 2015), the tidal amplitudes and ranges remain relatively consistent throughout the year.

Typhoons and other severe weather events also have a profound impact on the tidal and wave dynamics in the VES. These high-energy events can generate large, destructive waves and storm surges, which can significantly alter the seafloor morphology and sediment transport patterns (Gong et al., 2007; Zheng and Tang, 2007). The interaction between these extreme weather events and the complex bathymetry of the VES can also lead to the generation of large amplitude internal waves, further complicating the energy regime in the region.
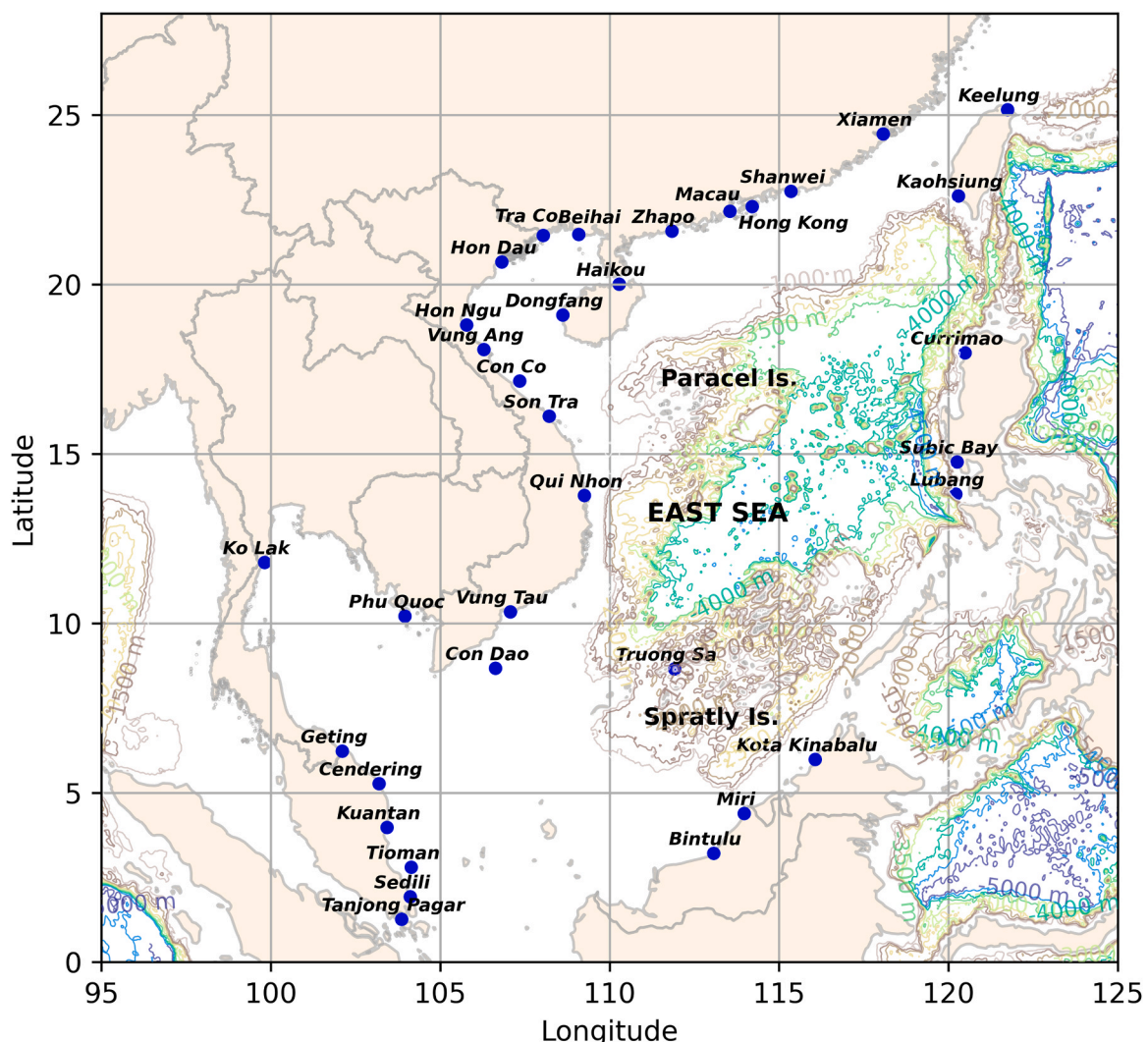

Fig. 1. Geographical distribution of tidal gauges in the Vietnam East Sea overlaid on bathymetry map (m) by GEBCO (2023) dataset.

2.2. Data

2.2.1. Semi-empirical tide model

This study assesses six prominent semi-empirical global ocean tide models: FES2014b, HAMTIDE12, GOT4.10c, DTU16, EOT20, and OSU12.V1. These models utilize varied numerical methods to integrate multi-mission satellite altimetry data for the extraction of tidal constituents and atlases. Table 2 presents essential information regarding the latest iterations of these semi-empirical tide models, encompassing developer details, spatial resolutions, programming environments, and the quantity of tidal constituents integrated. Subsequent sections provide detailed summaries of each model's characteristics and methods.

2.2.1.1. FES.
FES global tide atlases, developed since the mid-1990s, enhance altimetry mission accuracy in tidal correction. Using ensemble data assimilation to analyze large datasets (Lyard et al., 2021) (based on T-UGOm hydrodynamic tidal modeling and SpEnOI ensemble data assimilation), FES series includes FES94, FES95 (Shum et al., 1997), FES98, FES99 (Lefèvre et al., 2002), FES2002, FES2004, FES2012, and the latest FES2014. FES2014 significantly improves over FES2004 and FES2012, especially in coastal areas, due to flexible grids, prior hydrodynamic solutions, and ensemble assimilation. FES2014a is the first assimilation guess based on GOTv8 tidal loading data (Desai and Ray, 2014), leading to FES2014b's development. FES2014a was not widely distributed after its release as FES2014b with regular $1/16°$ resolution.

2.2.1.2. HAMTIDE.
Researchers from the University of Hamburg developed the HAMTIDE12 model, a global ocean barotropic data-assimilative model detailed in works by Zahel (1995) and Taguchi et al. (2014). It is based on linearized tidal hydrodynamic equations with simple harmonic time dependence. The model includes total loading and self-attraction effects (LSA or SAL) based on Hendershott (1972). Equations are numerically solved using finite difference methods. The conversion to the FES2004 grid involves reduced spacing in higher latitudes. GEBCO 1' bathymetry and EOT11a constraints within 74°N to 84°S are used. A direct optimization method minimizes a cost function with dynamical residual smoothing terms, addressing model deficiencies through numerical assimilation (Taguchi et al., 2014).

2.2.1.3. GOT.
The GOT model was developed at Goddard Space Flight Center, building on previous work by Schrama and Ray (1994) and Ray (1999). Like other models, it uses empirical harmonic analysis of satellite altimetry data compared to a predefined prior model, a composite of global and regional models merged at boundaries. GOT has a spatial resolution of 0.5°, the lowest among studied models, affecting near-coastal accuracy. For latitudes ± 66°, GOT relies solely on T/P satellite data with no Jason data (Ray, 2013), aiding consistency checks. For shallower oceanic regions and the deep waters beyond the 66° latitude mark, information from Geosat Follow-On, ERS-1, and ERS-2 satellites is utilized. Early ICESat data contribute, particularly in the Weddell and Ross seas. An iterative method by Cartwright and Ray (1991) addresses load tide, representing Earth's crustal deformation due to overlying ocean tide.

2.2.1.4. DTU.
The DTU10 global ocean tide model by the Technical University of Denmark incorporated FES2004 and the 'response method' proposed by Munk and Cartwright (1966). It derived harmonic coefficients from seventeen years of altimetry data, including TOPEX/-POSEIDON, Jason-1, and Jason-2. The latest version is DTU16. DTU16 estimated residual tides along satellite tracks using FES2012 and response analysis, then interpolated cosine and sine coefficients onto the FES2012 grid ($1/16° \times 1/16°$) using dynamic interpolation method based on tidal wavelength and water depth from DTU10 bathymetry. Additional data from two years of Jason-1 tandem missions and five years of Jason-2 missions expanded the dataset, enabling the separation of M_2 and S_2 tide constituents due to a three-year aliasing period. AltiKa data in the Arctic and ERS 1 data improved high-latitude accuracy.

2.2.1.5. EOT.
DGFI-TUM's empirical ocean tide models provide comprehensive global solutions for primary ocean tide constituents' amplitudes and phases. These models result from empirical analysis of satellite altimetry data from multiple missions involving residual harmonic analysis around reference models FES2014 or FES2004. EOT20 is the latest DGFI-TUM global ocean tide model, constructed using residual tidal analysis from multi-mission altimetry data spanning 1992–2019 (Hart-Davis et al., 2021). It relies on FES2014b as the reference model and covers from 66°S to 66°N, using FES2014b for higher latitudes. EOT20 provides data on seventeen tidal constituents, including 2N2, J_1, Ki, K_2, M_2, M_4, MF, MM, N_2, O_1, Pi, Qi, Si, S_2, SA, SSA, and T_2. The spatial resolution for ocean and load tide atlases is $1/8°$.

2.2.1.6. OSU.
OSU12, an ocean tide model from Ohio State University (Fok, 2012), uses an empirical approach and extended orthogonal representation of the response method (Groves and Reynolds, 1975) to determine ocean tides. A spatiotemporal weighting algorithm merges radar altimeter data from T/P, Jason-1, Geosat Follow-On (GFO), and Envisat, considering tidal aliasing, coverage, and accuracy. Data span from October 1992 to January 2009 within ± 66° latitude. The NAO99.b model by Matsumoto et al. (2000) is used for load tide corrections. OSU12v1.0 includes GOT4.7 model values beyond ± 66°. Efforts are underway to expand OSU12's coverage to include polar oceans. The model accounts for eight significant semidiurnal and diurnal tides, along with S_1 and M_4 tides.

2.2.2. Tidal gauges

Tidal gauge measurement is one of the primary methods for directly measuring sea level. Since the mid-19th century, tide gauges have been used to monitor sea level changes along continental coastlines and Mid-ocean Islands (Douglas, 2001; Jevrejeva et al., 2006; Ding et al., 2004). This study utilizes hourly tide data from the UHSLC tide gauge data archive (Caldwell et al., 2001) and the Vietnam Meteorological and Hydrological Administration. Out of numerous tide gauge stations in the VES region, only 34 stations were selected based on data length and quality. The locations of these chosen tide gauge stations can be seen in Fig. 1 and Table 3.

Table 2
Summary of semi-empirical tide models (source of datasets).

Model	Latest version	Developer	Resolution	Compiler environment	Number of Constituent
FES	FES2014b	NOVELTIS, CNES	1/16°	Fortran, C/C++	34
HAMTIDE	HAMTIDE12	Universitat Hamburg	1/8°	Fortran	8
GOT	GOT4.10C	Goddard Space Flight Center	1/2°	Fortran	10
DTU	DTU16	DTU space, TU Denmark	1/8°	Fortran	8
EOT	EOT20	DGFI-TUM	1/8°	Python, R, Matlab	17
OSU12	OSU12.V1	Ohio State University	1/4°	Fortran	8

Table 3

Tidal gauge locations in the VES analyzed in this study.

No.	Station	Latitude	Longitude	Country	Period	
					Begin	End
1	Cendering	5.27	103.19	Malaysia	11/1/1984	11/30/2015
2	Kuantan	3.98	103.43	Malaysia	12/22/1983	12/31/2015
3	Tioman	2.81	104.14	Malaysia	11/13/1985	12/31/2015
4	Sedili	1.93	104.12	Malaysia	12/23/1986	12/9/2015
5	Geting	6.23	102.11	Malaysia	12/17/1986	12/31/2015
6	Kota Kinabalu	5.98	116.07	Malaysia	6/24/1987	12/31/2015
7	Bintulu	3.22	113.07	Malaysia	5/1/1992	12/7/2015
8	Miri	4.39	113.97	Malaysia	12/22/1992	12/31/2014
9	Koh Lak	11.80	99.82	Thailand	1/1/1985	12/30/2019
10	Tanjong Pagar	1.26	103.85	Singapore	1/1/1988	12/30/2018
11	Subic Bay	14.77	120.25	Philippines (the)	2/28/2007	12/31/2018
12	Currimao	17.99	120.49	Philippines (the)	10/10/2009	12/31/2018
13	Lubang	13.82	120.21	Philippines (the)	6/12/2010	12/31/2018
14	Kaohsiung	22.62	120.29	Taiwan	1/2/1980	12/30/2016
15	Keelung	25.16	121.75	Taiwan	1/1/1980	12/30/2016
16	Xiamen	24.45	118.07	China	1/1/1954	12/30/1997
17	Zhapo	21.58	111.83	China	1/1/1975	12/30/1997
18	Beihai	21.48	109.08	China	1/1/1975	12/30/1997
19	Dongfang	19.10	108.62	China	1/1/1975	12/30/1997
20	Haikou	20.02	110.28	China	1/1/1976	12/30/1997
21	Shanwei	22.75	115.35	China	1/1/1975	12/31/1997
22	Macau	22.17	113.55	China	1/1/1978	5/30/1985
23	Hong Kong	22.30	114.20	China	1/1/1986	12/30/2018
24	Hon Dau	20.67	106.82	Vietnam	1/1/1960	12/31/2007
25	Tra Co	21.45	108.04	Vietnam	1/1/2020	10/31/2022

Table 3 (*continued*)

No.	Station	Latitude	Longitude	Country	Period	
					Begin	End
26	Hon Ngu	18.80	105.77	Vietnam	1/1/1999	12/31/2019
27	Vung Ang	18.08	106.28	Vietnam	9/4/1996	8/31/1997
28	Con Co	17.16	107.35	Vietnam	6/1/1980	11/30/2013
29	Son Tra	16.11	108.22	Vietnam	1/1/2015	12/31/2017
30	Qui Nhon	13.78	109.26	Vietnam	10/20/2007	12/30/2018
31	Vung Tau	10.34	107.07	Vietnam	10/16/2007	12/31/2018
32	Con Dao	8.68	106.63	Vietnam	1/1/1997	12/31/2017
33	Phu Quoc	10.22	103.96	Vietnam	1/1/2015	12/31/2022
34	Truong Sa	8.65	111.91	Vietnam	1/1/2005	12/31/2022

2.3. Validation method

The accuracy of model data for the VES region is examined by comparing them to tidal gauge measurements. These data sources encompass analysis of eight primary tidal constituents, including diurnal (K_1, O_1, P_1, Q_1) and semidiurnal (M_2, S_2, N_2, K_2) components. Decomposing tides into several harmonic constituents helps clarify the non-linearity of tidal forces in these areas (Mitra et al., 2022). The agreement between these data sources and tidal gauge measurements is further assessed using the root mean square deviations (RMSD) statistical metric, as shown in Eq. (1):

$$\text{RMSD} = \sqrt{\frac{\Sigma(X_1 - X_2)^2}{N}} \tag{1}$$

where X_1 and X_2 are the tidal harmonics from in-situ and model data, respectively, and N is the length of the times series.

Furthermore, the Taylor diagram (Taylor, 2001) is used to evaluate the credibility of the employed data sources. These diagrams present a graphical method to quantify the similarity between the data and observations in terms of correlation, centered root-mean-square difference, and standard deviations (Intergovernmental Panel on Climate Change (IPCC), 2001). The Taylor diagram analysis is particularly useful for assessing the comparative effectiveness of different tidal models, such as FES, DTU, EOT, GOT, HAMTIDE, and OSU against the reference tide gauge data. This method allows for a comprehensive evaluation of the various data sources and their ability to capture the tidal dynamics in the VES region, which is essential for assessing the tidal energy potential.

2.4. Calculating tidal energy potential

Tidal energy is a promising renewable resource that can be harnessed to generate electricity. Tidal movements present two exploitable energy forms: kinetic energy generated by the tidal current's motion and potential energy from the cyclic rise and fall of the tide (Rourke et al., 2009). The potential energy can be calculated based on the work required to lift the mass of water above the ocean's surface. The tidal potential energy can be expressed as Eq. (2) (Gorlov, 2009) below:

$$E = g\rho A \int zdz = 0.5g\rho Ah^2 \tag{2}$$

where E is the potential energy (J), g is the acceleration of gravity (9.8 m/s^2), p is the density of seawater, (approximately 1025 kg/m^3), A is the area of the relevant sea under consideration (m^2), z is the ocean surface's vertical position (unit: m), and h is the tide amplitude (m). Taking an average $(g\rho) = 10.15$ kN m^{-3} for seawater (Gorlov, 2009), the tidal potential energy per square meter of ocean surface for a complete tide cycle can be calculated as:

$$E = 1.4h^2 \tag{3}$$

This equation provides a straightforward method to estimate the theoretical tidal energy potential based on the tide amplitude in a given location (Rourke et al., 2009). Similar studies have employed this approach to assess the tidal energy potential in various coastal regions. For example, Yusoff et al. (2015) used Eq. (2) to estimate the tidal energy potential in the coastal regions of Malaysia, considering the tide range and bathymetric data. Their results showed that the theoretical tidal energy potential in the region was significant, with the potential to generate a substantial amount of electricity. In another study, Samrat (2013) applied the same methods to evaluate the tidal energy potential along the coasts of Bangladesh. The author found that certain locations, such as the Petenga and the Sandwip, had high tidal energy potential due to their favorable tide ranges and bathymetric conditions.

3. Results

3.1. Validation results

The RMSD analysis (Table 4) shows FES2014, DTU16, and EOT20 models exhibit the best performance in representing tidal dynamics in the VES region. The RMSD values show the average deviations between tide predictions from semi-empirical models and observed data across all available tide gauges for each tidal constituent. FES2014 has the lowest mean RMSD of 2.27 cm, indicating closest agreement with tide gauge data. DTU16 and EOT20 models have higher mean RMSD values, suggesting limitations in capturing complex VES tidal processes, particularly in coastal areas. The number of stations with RMSD ≤ 2 cm further supports FES2014, DTU16, and EOT20's superior performance (Fig. 2), indicating reliable tidal predictions across the VES, crucial for assessing tidal energy potential (Yusoff et al., 2015).

The Taylor diagram analysis, presented in Fig. 3, corroborates the RMSD-based conclusions, highlighting the strong performance of FES2014, DTU16, and EOT20. Across most tidal constituents, these models exhibit correlation coefficients exceeding 0.9, indicating a high degree of agreement with the observed tidal patterns. FES2014 displays its highest correlations for constituents M_2, N_2, P_1, and Q_1, demonstrating its ability to capture the dominant semi-diurnal and diurnal tidal components in the VES. Conversely, for constituents K_1, O_1, and S_2, the DTU16 model achieves the highest correlations. Additionally, EOT20 stands out in its ability to capture the K_2 constituent.

An independent evaluation by Hart-Davis et al. (2021), using 1226 tide gauges from the TICON dataset further validates the models' performance. EOT20 reduces the RMS for the M2 tidal constituent by 0.3 cm compared to FES2014b, the next best-performing model. EOT20 and FES2014b exhibit no more than 1 mm RMS differences for the remaining tidal constituents. This improvement by EOT20 over FES2014b is particularly pronounced in coastal areas. Overall, the evaluation by Hart-Davis et al. (2021) establishes EOT20 as yielding the most favorable results globally, followed by FES2014b and DTU16. However, in the present regional investigation in the VES, FES2014b exhibits stronger alignment with tidal station measurements compared to EOT20.

3.2. Tidal amplitude

The VES, while geographically semi-enclosed, is characterized by complex hydrodynamics that include a strong throughflow. This dynamic system is influenced by its intricate coastline geometry, variations in bathymetry, and significant interaction with the Western Pacific Ocean through the Luzon Strait, acting as a major heat and freshwater conveyor in the region. Tidal amplitudes for the VES region were calculated using the FES2014 global tidal constituent dataset. The process involved first predicting tidal levels at each location, and then identifying the highest and lowest tides from these predictions. The tidal amplitude was defined as half the difference between these extreme levels. As illustrated in Fig. 4 and Table 5, the FES2014 model reveals three emerging hotspots exhibiting substantial tidal amplitudes The region south of Guangdong near Anpu Gang (China) with 326.2 cm, the area south of Vietnam near Bac Lieu with 217.5 cm, and the Batang Lupar estuary (Malaysia) with 255.09 cm. Among these locations, the Anpu Gang experiences the highest tidal amplitude.

The tidal dynamics in the VES are characterized by a mixed but predominantly semi-diurnal tidal regime, as evidenced by the FES2014 model (Fig. 5). The M_2 tidal constituent generally exhibits larger amplitudes than the diurnal K_1 constituent across most of the VES, except for the Gulf of Tonkin near Anpu Gang, where the diurnal component is more energetic.

3.3. Potential energy

The spatial distribution of tidal energy potential across the VES domain, computed using tidal amplitudes from the FES2014 dataset and the potential energy equation (Eq. (3)), reveals three notable hotspots with significantly higher potential energy levels (Fig. 6). These hotspots correspond to the areas with the largest tidal amplitudes: Anpu Gang (14.9 Wh/m^2), Bac Lieu (6.62 Wh/m^2), and the Batang Lupar estuary (9.11 Wh/m^2). Among these, the Anpu Gang emerges as the most promising site for tidal energy extraction, boasting the highest potential energy value within the VES region. Specific reference points around the VES, such as the Sittang River (13.64 Wh/m^2), Rokan River (11.48 Wh/m^2), and Dongwu Yang (18.20 Wh/m^2), exhibit potential energy values similar to or exceeding those of the identified VES hotspots.

Table 4

The RMSD (cm) of the tidal constituents for semi-empirical tide models, averaged across all tide gauges.

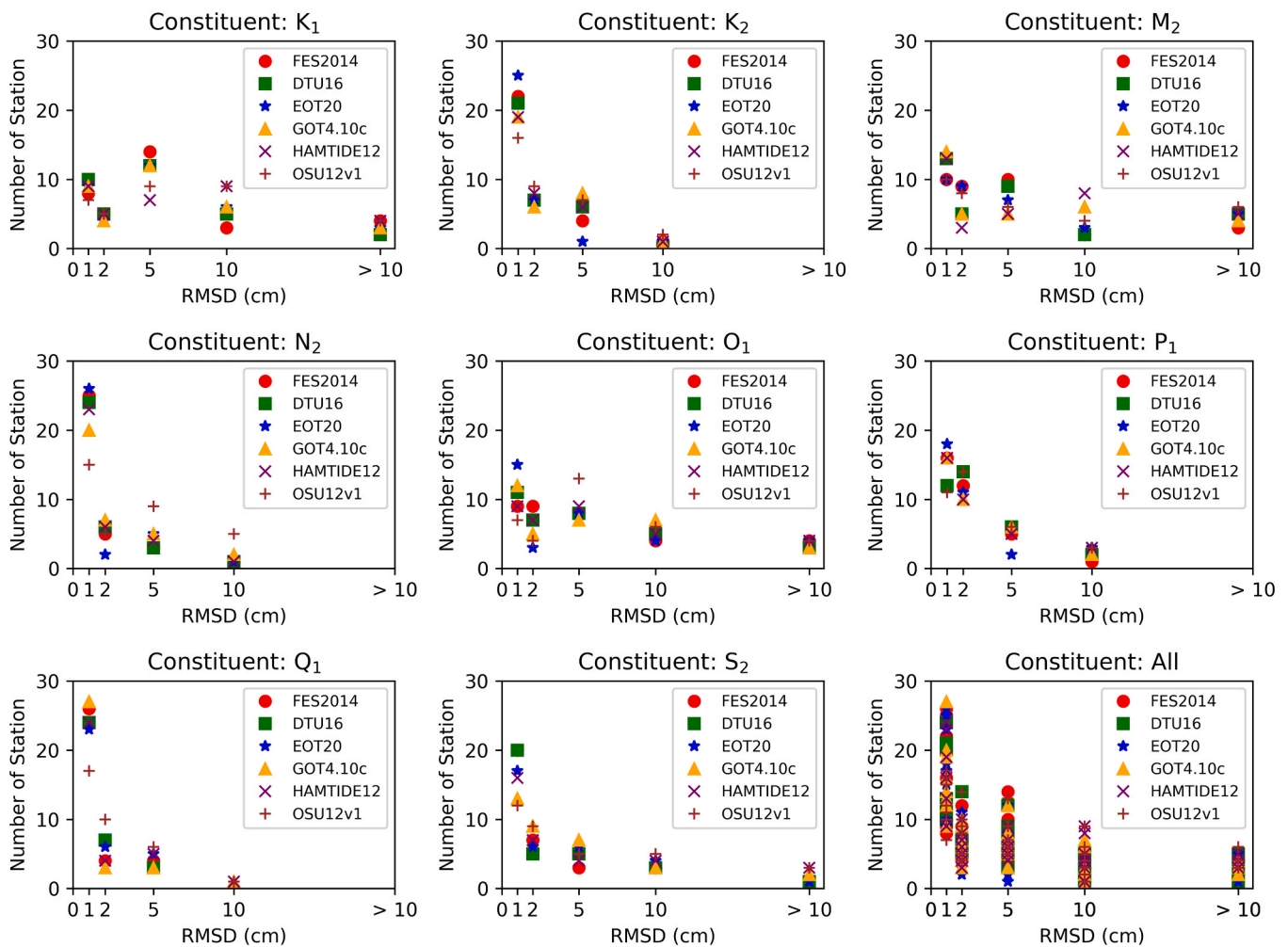| Constituent	FES2014	DTU16	EOT20	GOT4.10c	HAMTIDE12	OSU12v1
K_1	4.11	3.37	4.62	4.11	5.04	5.28
O_1	3.70	3.46	3.88	3.98	4.58	4.99
P_1	1.31	1.74	1.46	1.42	1.57	1.82
Q_1	0.84	0.84	0.96	0.94	1.10	1.32
M_2	4.19	4.88	4.64	5.64	6.40	6.01
K_2	1.08	1.19	0.82	1.45	1.26	1.55
N_2	0.97	1.21	1.09	1.41	1.13	2.22
S_2	1.93	1.99	2.39	2.71	2.99	3.35
Mean of all	2.27	2.34	2.48	2.71	3.01	3.32

Fig. 2. Scatter diagram of root mean square deviation (RMSD) and number of stations for semi-empirical tide models.

4. Discussion

4.1. Model performance

FES2014's superior performance is attributed to its advanced data assimilation scheme with ensemble techniques and flexible grid resolutions for capturing complex coastal dynamics (Stammer et al., 2014; Taguchi et al., 2014). FES2014 blends tidal information from hydrodynamic models, satellite altimetry, and in-situ observations, improving tidal pattern representation (Lyard et al., 2021). Its flexible grid resolution better resolves the intricate VES bathymetry and coastal features, which significantly influence tidal propagation and energy dissipation (Morozov, 1995; Egbert and Ray, 2000; Niwa and Hibiya, 2004; Zu et al., 2008). FES2014 aims to improve water level modeling in shoreline and shallow water areas compared to other models (Khomsin et al., 2021). Its integration of satellite altimetry and updated ITRF standards facilitated more precise regional and coastal modeling, improving global oceanic calibration standards (Piccioni et al., 2018). In contrast, DTU16 and EOT20 models show limitations in capturing complex VES tidal processes, particularly in coastal areas. This difference is attributed to the hydrodynamic aspects of the models. FES2014's T-UGOm framework solves Navier–Stokes equations under the Boussinesq approximation with 2D/3D flexible grid (Stammer et al., 2014), better representing the complex VES bathymetry and coastal geometries that influence tidal propagation and energy dissipation (Gan et al., 2006; Morozov, 1995; Zu et al., 2008). DTU16 and EOT20 rely more on empirical methods using satellite altimetry data and response analysis techniques (Cheng and

Andersen, 2011), potentially overlooking intricate hydrodynamic processes like the effects of steep continental shelf and numerous islands in the VES (Ye and Robinson, 1983).

The Taylor diagram analysis aligns with the findings of previous studies, such as Stammer et al. (2014), who emphasized the importance of advanced assimilation techniques in improving the accuracy of global tide models. The high correlations for constituents M_2, N_2, P_1, and Q_1 in FES2014 demonstrate its ability to capture the dominant semi-diurnal and diurnal tidal components in the VES, consistent with the region's tidal dynamics described by Sergeev (1964). DTU16's proficiency in reproducing K_1, O_1, and S_2 components can be attributed to its reliance on a comprehensive dataset of satellite altimetry observations (Munk and Cartwright, 1966). EOT20's strong performance in capturing the K_2 constituent can be linked to its usage of the FES2014 solution as a reference, allowing it to better resolve the complex tidal interactions in the VES, as highlighted by Egbert and Ray (2000) and Niwa and Hibiya (2004). While EOT20 generally demonstrates superior performance on a global scale, it falls short in certain regional studies like the VES, primarily due to inferior resolution and the absence of in-situ measurements incorporated for this region. Consequently, FES2014b emerges as the preferred dataset for evaluating tidal energy potential in the VES area.

4.2. Tidal dynamics and energy potential

The tidal hydrodynamics in the VES are influenced by its semi-enclosed nature, complex coastline, varying bathymetry, and
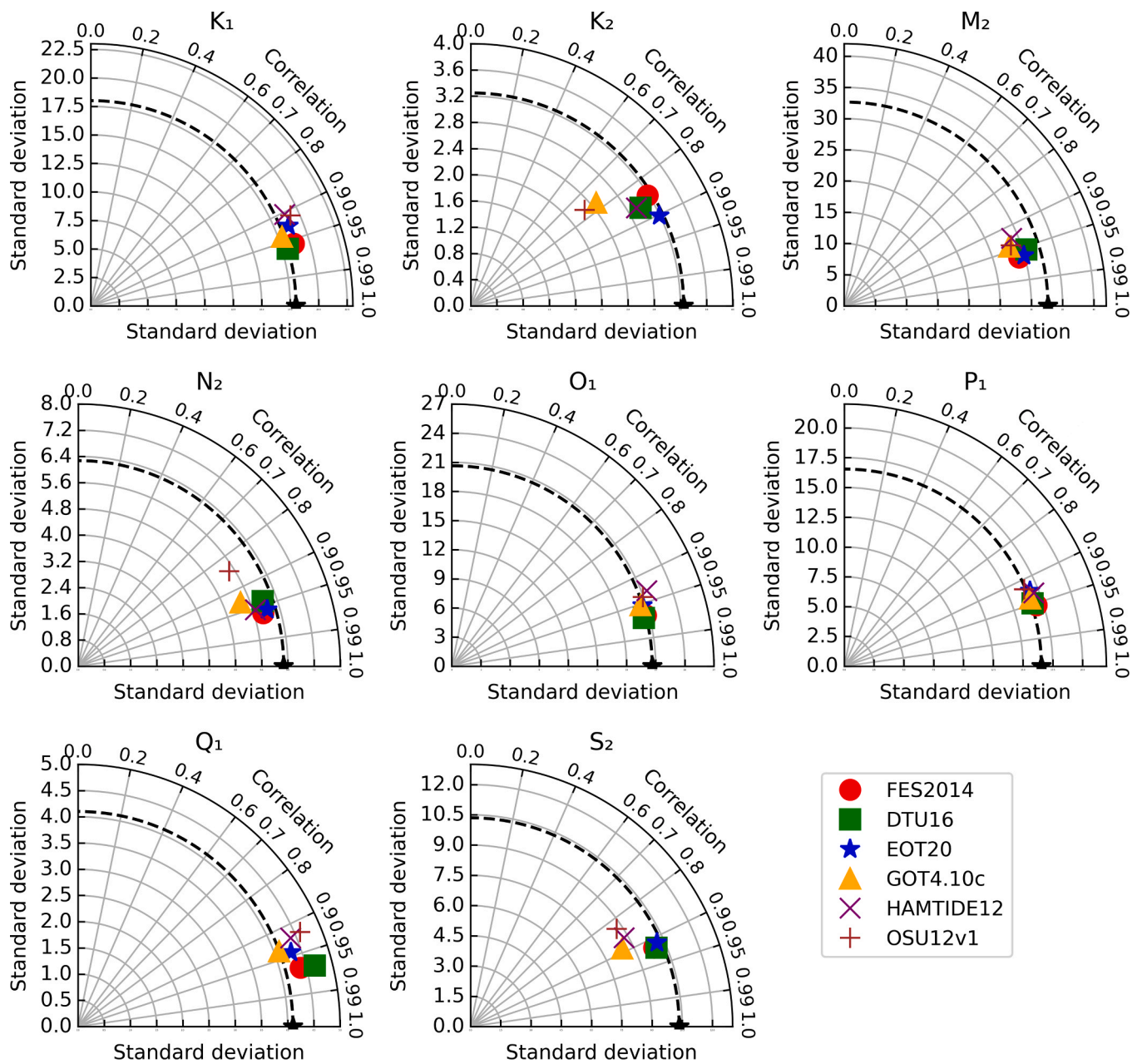
Fig. 3. Taylor diagram between tidal gauges and semi-empirical tide models.

interaction with the Western Pacific Ocean via the Luzon Strait. As the tidal wave propagates from the Pacific into the VES, it undergoes deformation, reflection, and resonance due to the combined effects of topographic features and basin modes (Ye and Robinson, 1983). These processes contribute to the formation of amphidromic systems and the complex spatial patterns observed in tidal amplitudes and phases throughout the VES. The tidal data provided by FES2014 demonstrate a notable consistency with findings from prior studies conducted by Fang et al. (1999) and Zu et al. (2008), particularly in areas with the most significant tidal amplitudes. These locations typically correspond to points with the highest potential energy within the VES. Notably, these regions are characterized by coastal areas featuring considerable shoaling and constriction effects, accompanied by shallower continental shelves and the presence of straits or coastlines with a concave shape. This circumstance contributes to amplifying the M_2 tide. Ye and Robinson (1983) argued that the actual diurnal energy dissipation is much greater than the semi-diurnal energy dissipation, which partially

explains the prevalence of the semi-diurnal component (M_2) in the tidal dynamics of the VES, influencing the distribution of potential energy within the region, as indicated by the FES2014 data. While the moderate tidal amplitudes observed in the broader VES region may limit the potential for large-scale tidal power development, the identified hotspots, particularly the Batang Lupar estuary, warrant further investigation for localized tidal energy projects. The intricate hydrodynamics and energetics of the VES tidal system present opportunities for advanced modeling efforts to enhance our understanding and optimize tidal energy extraction in this region.

4.3. Potential energy assessment

In a global context, the potential tidal energy in the VES can be characterized as moderate to low compared to regions with exceptionally large tidal ranges and amplitudes, such as the Bay of Fundy (Canada), the English Channel, and the Pentland Firth (UK), where potential
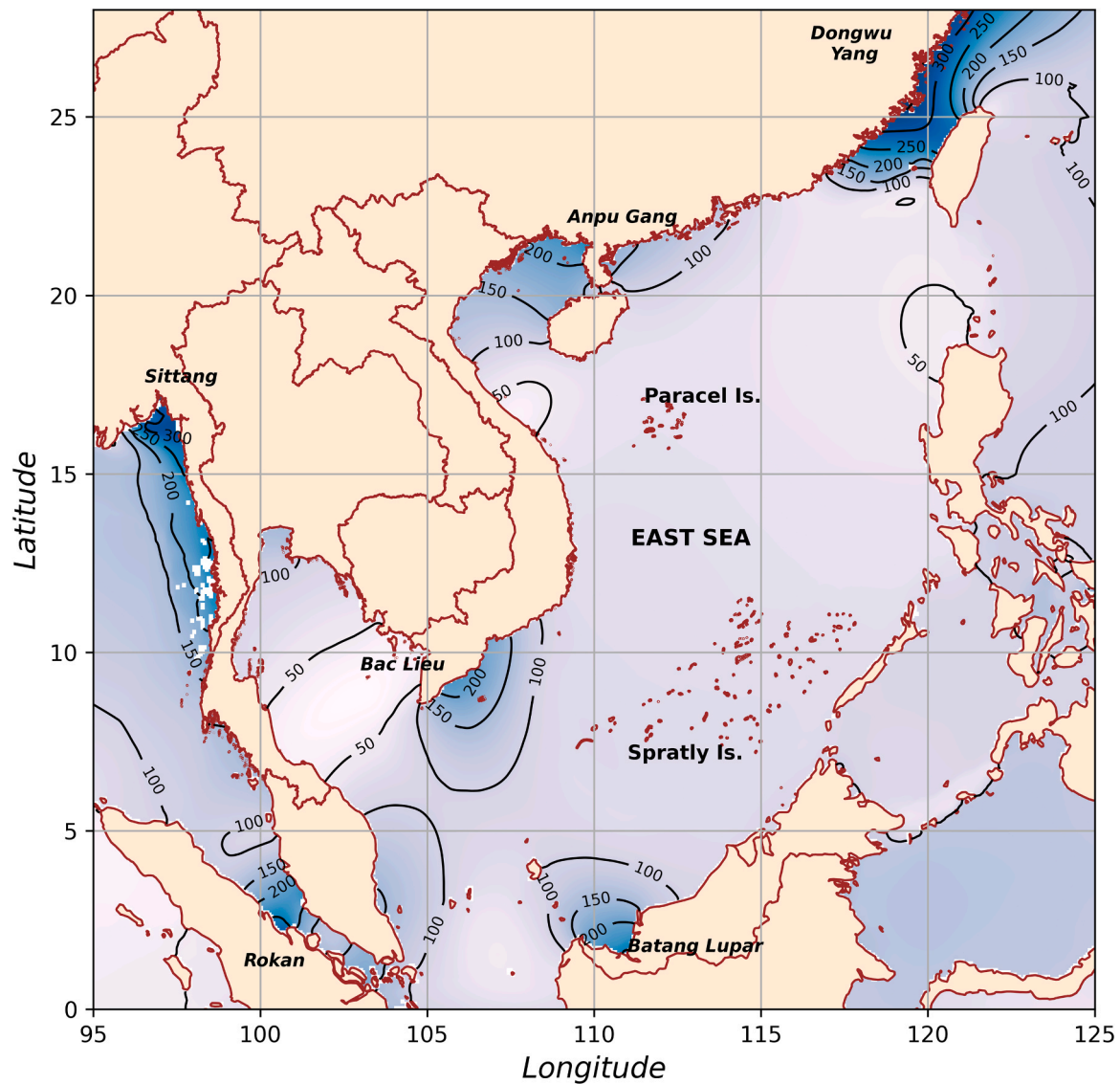
Fig. 4. Average predicted tidal amplitude in VES (calculated based on FES2014).

Table 5
Highest tidal amplitude at several sites in the world and the VES from FES2014.

Region	Country	Site	Amplitude (cm)
World	France	La Rance	628.73
	China	Jiangxia	379.35
	Canada	Annapolis	484.29
	South Korea	Sihwa Lake	518.66
Around VES	Myanmar	Estuary of Sittang river (Gulf of Martaban)	312.19
	Indonesia	Estuary of Rokan river	286.33
	China	Dongwu Yang	360.52
VES	China	Anpu Gang	326.20
	Vietnam	Bac Lieu	217.51
	Malaysia	Batang Lupar estuary	255.09

energy values often exceed 50 Wh/m^2 (Johnston et al., 2013). Conversely, enclosed oceans with relatively smaller tidal amplitudes, like the Mediterranean Sea, generally have lower potential energy levels compared to the VES (Zhang et al., 2014). The geographic areas within the VES region exhibiting the highest potential energy levels (Anpu Gang, Bac Lieu, and the Batang Lupar estuary) have potential energy values lower than those observed at the Jiangxia tidal power plant (20.15 Wh/m^2). The Jiangxia power plant has an average global capacity of 3.9 MW at a tidal amplitude of 379.35 cm. Neill et al. (2018) identify global sites where tidal range energy projects are technically feasible, emphasizing locations with tidal ranges between 4.5 and 12 m, equating to tidal amplitudes of 225–600 cm. Some suitable sites in South Korea (Cheonsu - 225 cm, Garorim - 235 cm), India (Gulf of Kutch - 265 cm) or the UK (Conwy - 260 cm) have tidal amplitudes comparable to Bac Lieu or Batang Lupar. Our proposed sites—Anpu Gang (326.2 cm), Bac Lieu (217.51 cm), and Batang Lupar (255.09 cm)—fall within this range, indicating significant tidal energy potential based on average tidal amplitude. While no universal threshold is specified in the literature, the consistent tidal amplitude range in viable locations serves as a practical benchmark for evaluating potential tidal power plant sites.

This comparison indicates that the tidal energy development potential in the identified VES hotspots is not negligible, although further assessments are necessary. It is essential to acknowledge that tidal energy encompasses both potential and kinetic energy components, and relying solely on assessing potential energy for determining tidal energy provisioning at a given location may not provide a complete picture. However, such quantification remains a pivotal reference parameter in selecting optimal sites and designing future tidal energy plants. Despite
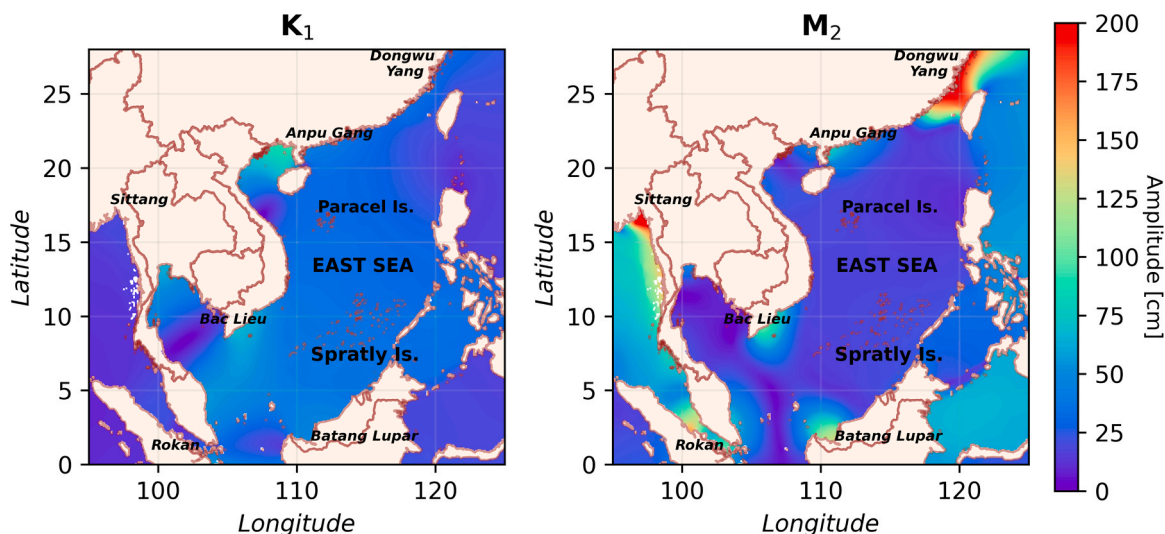
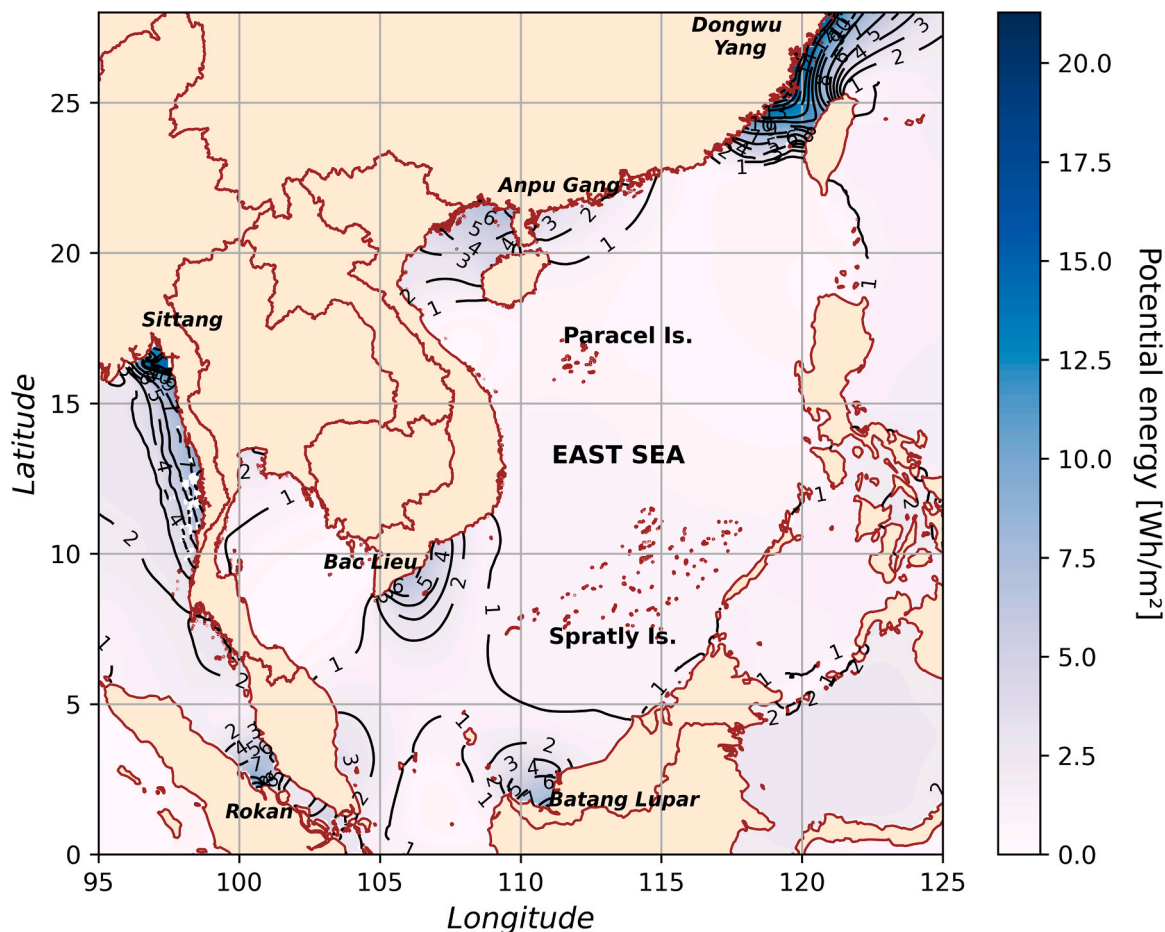**Fig. 5.** K_1 and M_2 amplitude from FES2014.

Fig. 6. Potential energy in Vietnam East Sea.

the moderate potential energy levels observed in the VES hotspots, these areas still represent a valuable renewable energy resource worth exploring for potential development. The localized nature of these hotspots presents opportunities for small to medium-scale tidal energy projects tailored to specific coastal regions and communities. Moreover, the identified hotspots can serve as initial targets for more detailed site-specific resource assessments, considering local bathymetry, flow

velocities, environmental constraints, and socio-economic factors. The potential tidal energy values obtained in this study align with previous assessments conducted in the VES region, such as those by Tong et al. (2010) and Johnston et al. (2013), further validating the findings and supporting the conclusion that while the VES may not be suitable for large-scale tidal energy projects comparable to global leaders, it does offer promising opportunities for smaller, localized tidal energy

developments.

5. Conclusion

This comprehensive study assessed and validated prominent semi-empirical global ocean tide models against an extensive tide gauge network in the VES region. Evaluation results unveiled the superior performance of the FES2014, DTU16, and EOT20 models in capturing the intricate tidal dynamics within the semi-enclosed basin of the VES. Notably, the FES2014 model demonstrated the closest agreement with tide gauge measurements, credited to its advanced data assimilation techniques, flexible grid resolutions, and comprehensive representation of hydrodynamic processes influenced by the region's complex bathymetry and coastal geometry.

By leveraging the capabilities of the FES2014 model, the study identified the semi-diurnal component (M_2) as the most prevalent tidal constituent in the VES, significantly influencing potential energy distribution within the region. Furthermore, three emerging hotspots characterized by substantial tidal amplitudes were pinpointed: the Batang Lupar estuary (Malaysia, 255.09 cm), Anpu Gang (China, 326.2 cm), and Bac Lieu (Vietnam, 217.51 cm). Among these, the Anpu Gang stood out with the highest potential tidal energy of 14.90 Wh/m^2, positioning it as the most promising site for localized tidal power development within the VES. While the observed moderate tidal amplitudes and potential energy levels may not accommodate large-scale tidal power plants comparable to globally renowned sites, these identified hotspots warrant further exploration for small-to-medium scale projects tailored to local coastal regions. This localized approach, coupled with the intricate hydrodynamics of the VES, underscores the necessity for advanced modeling to optimize tidal energy extraction efficiently.

While acknowledging that assessing potential energy alone presents an incomplete picture, as tidal energy encompasses both potential and kinetic components, quantifying potential energy remains paramount for site selection and plant design. The moderate yet promising potential observed in the identified VES hotspots represents a valuable renewable resource worthy of exploration for sustainable tidal energy solutions. This foundational assessment, employing state-of-the-art models and rigorous validation, underscores the moderate tidal energy potential inherent in the VES. These findings lay the groundwork for targeted investigations and the development of localized tidal power projects, thereby contributing to the region's sustainable energy transition.

Although tidal energy development in the VES is still in its nascent stages, the outlook for this renewable energy source is promising. As tidal energy generation technology continues to advance, the VES has the potential to emerge as a significant source of clean and renewable energy, further bolstering the global transition towards sustainable energy solutions.

CRediT authorship contribution statement

Long Trinh-Tuan: Writing – review & editing, Validation, Methodology. **Quan Tran-Anh:** Writing – review & editing, Validation, Methodology. **Tuan Nguyen-Le:** Writing – review & editing, Supervision, Funding acquisition, Formal analysis, Conceptualization. **Loc Nguyen-Xuan:** Writing – original draft, Visualization, Validation, Methodology, Data curation, Conceptualization.

Supplementary information

Not applicable.

Declaration of Competing Interest

The authors have no competing interests to declare that are relevant to the content of this article.

Data availability

Data will be made available on request.

References

Abd Rahim, M.W., Rahman, A.A., Izham, M., Amin, N.A.M., 2023. Tidal Energy in Malaysia: an overview of potentials, device suitability, issues and outlook. Reg. Stud. Mar. Sci. 61, 102853. https://doi.org/10.1016/j.rsma.2023.102853.

Amedo-Repollo, C.L., Flores-Vidal, X., Chavanne, C., Villanoy, C.L., Flament, P., 2021. Barotropic and baroclinic tides in Panay Strait, Philippines. Reg. Stud. Mar. Sci. 41, 101612. https://doi.org/10.1016/j.rsma.2021.101612.

Bae, Y.H., Kim, K.O., Choi, B.H., 2010. Lake Sihwa tidal power plant project. Ocean Eng. 37 (5–6), 454–463. https://doi.org/10.1016/j.oceaneng.2010.01.015.

Bernshtein, L.B., 1972. Kislaya Guba experimental tidal power plant and problem of the use of tidal energy. In: Gray, T.J., Gashus, O.K. (Eds.), Tidal Power. Springer US, pp. 215–238. https://doi.org/10.1007/978-1-4613-4592-3_6.

Bui, N.Q., 2010. Morphology of the Eastern Scheldt ebb tidal delta. ⟨https://repository.tudelft.nl/islandora/object/uuid%3A995b9189-5a6e-430f-9abd-99355dae120e⟩.

Caldwell, P.C., Merrifield, M.A., Thompson, P.R., 2001. Sea level measured by tide gauges from global oceans as part of the Joint Archive for Sea Level (JASL) since 1846. [dataset]. [object Object]. NOAA National Centers for Environmental Information. Dataset. ⟨https://doi.org/10.7289/v5v40s7w⟩.

Cartwright, D.E., Ray, R.D., 1991. Energetics of global ocean tides from Geosat altimetry. J. Geophys. Res.: Oceans 96 (C9), 16897–16912. https://doi.org/10.1029/91JC01059.

Charlier, R., 2007. Forty candles for the Rance River TPP tides provide renewable and sustainable power generation. Renew. Sustain. Energy Rev. 11 (9), 2032–2057. https://doi.org/10.1016/j.rser.2006.03.015.

Chen, G., Gan, J., Xie, Q., Chu, X., Wang, D., Hou, Y., 2012. Eddy heat and salt transports in the South China Sea and their seasonal modulations. J. Geophys. Res. Atmos. 117 (C5). https://doi.org/10.1029/2011jc007724.

Cheng, Y., Andersen, O.B., 2011. Multimission empirical ocean tide modeling for shallow waters and polar seas. J. Geophys. Res.: Oceans 116 (C11), 2011JC007172. https://doi.org/10.1029/2011JC007172.

Dai, Y., Ren, Z., Wang, K., Li, W., Li, Z., Yan, W., 2018. Optimal sizing and arrangement of tidal current farm. IEEE Trans. Sustain. Energy 9, 168–177. https://doi.org/10.1109/TSTE.2017.2719042.

Desai, S.D., Ray, R.D., 2014. Consideration of tidal variations in the geocenter on satellite altimeter observations of ocean tides. Geophys. Res. Lett. 41 (7), 2454–2459. https://doi.org/10.1002/2014GL059614.

Ding, X., Zheng, D.W., Wong, W.T., Li, K., Zhong, P., Chen, W., 2004. Recent sea level variations in Southern China from tide gauge observations. APSG Symp. 126–136.

Domenech, J., Eveleigh, T., Tanju, B., 2018. Marine Hydrokinetic (MHK) systems: using systems thinking in resource characterization and estimating costs for the practical harvest of electricity from tidal currents. Renew. Sustain. Energy Rev. 81, 723–730. https://doi.org/10.1016/j.rser.2017.07.063.

Douglas, B.C., 2001. Chapter 3 sea level change in the era of the recording tide gauge. In: International Geophysics, vol. 75. Elsevier, pp. 37–64. ⟨https://doi.org/10.1016/S0074-6142(01)80006-1⟩.

Egbert, G.D., Ray, R.D., 2000. Significant dissipation of tidal energy in the deep ocean inferred from satellite altimeter data. Nature 405 (6788), 775–778. https://doi.org/10.1038/35015531.

Fang, G., Kwok, Y.-K., Yu, K., Zhu, Y., 1999. Numerical simulation of principal tidal constituents in the South China Sea, Gulf of Tonkin and Gulf of Thailand. Cont. Shelf Res. 19 (7), 845–869. https://doi.org/10.1016/S0278-4343(99)00002-3.

Feng, H., Feng, X., Feng, W., Zhang, W., 2021. Sensitivity of tides and tidal components to sea-level-rise in the Radial Sand Ridges. Reg. Stud. Mar. Sci. 47, 101918. https://doi.org/10.1016/j.rsma.2021.101918.

Fok, H.S., 2012. Ocean tides modeling using satellite altimetry. The Ohio State University. ⟨https://etd.ohiolink.edu/acprod/odb_etd/etd/r/1501/10?clear=10&p10_accession_num=osu1354040445⟩.

Gan, J., Li, H., Curchitser, E.N., Haidvogel, D.B., 2006. Modeling South China Sea circulation: response to seasonal forcing regimes. J. Geophys. Res.: Oceans 111 (C6), 2005JC003298. https://doi.org/10.1029/2005JC003298.

Gong, W., Shen, J., Reay, W.G., 2007. The hydrodynamic response of the york river estuary to tropical cyclone isabel, 2003. Estuar. Coast. Shelf Sci. 73 (3), 695–710. https://doi.org/10.1016/j.ecss.2007.03.012.

Gorlov, A.M., 2009. Tidal energy. In: Thorpe, S.A. (Ed.), Elements of Physical Oceanography. Elsevier Academic Press, pp. 103–109.

Groves, G.W., Reynolds, R.W., 1975. An orthogonalized convolution method of tide prediction. J. Geophys. Res. 80 (30), 4131–4138. https://doi.org/10.1029/JC080i030p04131.

Hart-Davis, M.G., Piccioni, G., Dettmering, D., Schwatke, C., Passaro, M., Seitz, F., 2021. EOT20: a global ocean tide model from multi-mission satellite altimetry. Earth Syst. Sci. Data 13 (8), 3869–3884. https://doi.org/10.5194/essd-13-3869-2021.

Hendershott, M.C., 1972. The effects of solid earth deformation on global ocean tides. Geophys. J. Int. 29 (4), 389–402. https://doi.org/10.1111/j.1365-246X.1972.tb06167.x.

Hu, Q., Huang, X., Zhang, Z., Zhang, X., Xu, X., Sun, H., Tian, J., et al., 2020. Cascade of internal wave energy catalyzed by eddy-topography interactions in the deep South China Sea. Geophys. Res. Lett. 47 (4). https://doi.org/10.1029/2019gl086510.

Huang, X., Huang, S., Zhao, W., Zhang, Z., Zhou, C., Tian, J., 2022. Temporal variability of internal solitary waves in the northern South China Sea revealed by long-term mooring observations. Prog. Oceanogr. 201, 102716.

Intergovernmental Panel on Climate Change (IPCC), 2001. Climate Change 2001: The Scientific Basis, Contribution of Working Group I to the Third Assessment Report of the Intergovernmental Panel on Climate Change. Cambridge University Press, Cambridge, United Kingdom and New York, NY, USA, p. 881.

Jevrejeva, S., Grinsted, A., Moore, J.C., Holgate, S., 2006. Nonlinear trends and multiyear cycles in sea level records. J. Geophys. Res.: Oceans 111 (C9), 2005JC003229. https://doi.org/10.1029/2005JC003229.

Jian-yu, H., Kawamura, H., Hua-sheng, H., Kobashi, F., Qiang, X., 2001. Tidal features in the China Seas and their adjacent sea areas as derived from TOPEX/POSEIDON altimeter data. Chin. J. Oceanol. Limnol. 19 (4), 293–305. https://doi.org/10.1007/BF02850732.

Johnston, T.M.S., Rudnick, D.L., Alford, M.H., Pickering, A., Simmons, H.L., 2013. Internal tidal energy fluxes in the South China Sea from density and velocity measurements by gliders. J. Geophys. Res.: Oceans 118 (8), 3939–3949. https://doi.org/10.1002/jgrc.20311.

Khomsin, Pratomo, D.G., Rohmawati, C.N., 2021. Analysis of accuracy comparison tidal global (FES2014, TPXO9) and regional (BIG Prediction) models to the existing tides in Surabaya and surrounding waters. IOP Conf. Ser.: Earth Environ. Sci. 936 (1), 012028. https://doi.org/10.1088/1755-1315/936/1/012028.

Kvale, E.P., 2006. The origin of neap–spring tidal cycles. Mar. Geol. 235 (1–4), 5–18. https://doi.org/10.1016/j.margeo.2006.10.001.

Lefèvre, F., Lyard, F.H., Provost, C.L., Schrama, E.J.O., 2002. Fes99: a global tide finite element solution assimilating tide gauge and altimetric information. J. Atmos. Ocean. Technol. 19 (9), 1345–1356. https://doi.org/10.1175/1520-0426(2002)019<1345:FAGTFE>2.0.CO;2.

Li, B., Wei, Z., Wang, X., Fu, Y., Fu, Q., Li, J., Lv, X., et al., 2020. Variability of coherent and incoherent features of internal tides in the North South China Sea. Sci. Rep. 10 (1). https://doi.org/10.1038/s41598-020-68359-7.

Li, M., 2021. Assessment and mitigation of environmental impacts from the bay of fundy tidal energy development, atlantic canada. MLWS. ⟨https://mlws.landfood.ubc.ca/all-projects/assessment-and-mitigation-of-environmental-impacts-from-the-bay-of-fundy-tidal-energy-development-atlantic-canada/⟩.

Lyard, F.H., Allain, D.J., Cancet, M., Carrère, L., Picot, N., 2021. FES2014 global ocean tide atlas: design and performance. Ocean Sci. 17 (3), 615–649. https://doi.org/10.5194/os-17-615-2021.

Mao, Q., Gao, Y., Fan, J., 2024. An integrated MCDM framework for tidal current power plant site selection based on interval 2-tuple linguistic. Reg. Stud. Mar. Sci. 74, 103518. https://doi.org/10.1016/j.rsma.2024.103518.

Matsumoto, K., Takanezawa, T., Ooe, M., 2000. Ocean tide models developed by assimilating TOPEX/POSEIDON altimeter data into hydrodynamical model: A global model and a regional model around Japan. Journal of oceanography 56, 567–581. https://doi.org/10.1023/A:1011157212596.

Mitra, A., Mandal, S., Shanas, P.R., Joseph, D., Yuvaraj, S., George, J., Aravind, P., Singh, J., Kumar, V.S., 2022. Variability in tidal harmonics of the coastal and estuarine waters of Goa during winter monsoon and spring inter-monsoon. Reg. Stud. Mar. Sci. 51, 102226. https://doi.org/10.1016/j.rsma.2022.102226.

Morozov, E.G., 1995. Semidiurnal internal wave global field. Deep Sea Res. Part I: Oceanogr. Res. Pap. 42 (1), 135–148. https://doi.org/10.1016/0967-0637(95)92886-C.

Munk, W.H., Cartwright, D.E., 1966. Tidal spectroscopy and prediction. Philos. Trans. R. Soc. Lond. Ser. A Math. Phys. Sci. 259 (1966), 533–581. https://doi.org/10.1098/rsta.1966.0024.

Nazri, N., Anuar, S., Basrawi, F., Shukrie, A., Aishah, S., 2018. Evaluation of potential sites for harnessing tidal energy around coastal area of Malaysia. MATEC Web Conf. 225, 06015. https://doi.org/10.1051/matecconf/201822506015.

Neill, S.P., Vögler, A., Goward-Brown, A.J., Baston, S., Lewis, M.J., Gillibrand, P.A., Waldman, S., Woolf, D.K., 2017. The wave and tidal resource of Scotland. Renew. Energy 114, 3–17. https://doi.org/10.1016/j.renene.2017.03.027.

Neill, S.P., Angeloudis, A., Robins, P.E., Walkington, I., Ward, S.L., Masters, I., Falconer, R., et al., 2018. Tidal range energy resource and optimization–past perspectives and future challenges. Renew. Energy 127, 763–778.

Neill, S.P., Hemer, M., Robins, P.E., Griffiths, A., Furnish, A., Angeloudis, A., 2021. Tidal range resource of Australia. Renew. Energy 170, 683–692. https://doi.org/10.1016/j.renene.2021.02.035.

Niwa, Y., Hibiya, T., 2004. Three-dimensional numerical simulation of M 2 internal tides in the East China Sea. J. Geophys. Res.: Oceans 109 (C4), 2003JC001923. https://doi.org/10.1029/2003JC001923.

Passaro, M., Cipollini, P., Vignudelli, S., Quartly, G.D., Snaith, H.M., 2014. ALES: a multi-mission adaptive subwaveform retracker for coastal and open ocean altimetry. Remote Sens. Environ. 145, 173–189. https://doi.org/10.1016/j.rse.2014.02.008.

Passaro, M., Nadzir, Z.A., Quartly, G.D., 2018. Improving the precision of sea level data from satellite altimetry with high-frequency and regional sea state bias corrections. Remote Sens. Environ. 218, 245–254. https://doi.org/10.1016/j.rse.2018.09.007.

Piccioni, G., Dettmering, D., Passaro, M., Schwatke, C., Bosch, W., Seitz, F., 2018. Coastal improvements for tide models: the impact of Ales retracker. Remote Sens. 10 (5), 700. https://doi.org/10.3390/rs10050700.

Rainville, L., Pinkel, R., 2006. Propagation of low-mode internal waves through the ocean. J. Phys. Oceanogr. 36 (6), 1220–1236. https://doi.org/10.1175/JPO2889.1.

Ray, R.D., 1999. A global ocean tide model from topex/poseidon altimetry: Got99. 2. ⟨https://ntrs.nasa.gov/citations/19990089548⟩.

Ray, R.D., 2013. Precise comparisons of bottom-pressure and altimetric ocean tides. J. Geophys. Res.: Oceans 118 (9), 4570–4584. https://doi.org/10.1002/jgrc.20336.

Rourke, F.O., Boyle, F., Reynolds, A., 2009. Renewable energy resources and technologies applicable to Ireland. Renew. Sustain. Energy Rev. 13 (8), 1975–1984. https://doi.org/10.1016/j.rser.2009.01.014.

Samrat, N.H., Mamun, N., Uddin, S.M., Islam, A., 2013. Case study: tidal current energy potential in Bangladesh. Int. Conf. Inform. Electron. Vis. (ICIEV) 2013, 1–5. https://doi.org/10.1109/ICIEV.2013.6572556.

Schrama, E.J.O., Ray, R.D., 1994. A preliminary tidal analysis of TOPEX/POSEIDON altimetry. J. Geophys. Res.: Oceans 99 (C12), 24799–24808. https://doi.org/10.1029/94JC01432.

Sergeev, J.N., 1964. The application of the method of marginal values for the calculation of charts of tidal harmonic constants in the South China Sea. Okeanologiia 4, 595–602 in Russian, English abstract.

Shao, M., Zhao, Y., Sun, J., Han, Z., Shao, Z., 2023. A decision framework for tidal current power plant site selection based on GIS-MCDM: a case study in China. Energy 262. https://doi.org/10.1016/j.energy.2022.125476.

Shetty, C., Priyam, A., 2022. A review on tidal energy technologies. Mater. Today: Proc. 56 (5), 2774–2779. https://doi.org/10.1016/j.matpr.2021.10.020.

Shuai, Y., Li, Q., Wu, Z., 2021. Biogeochemical responses to nutrient fluxes in the open South China Sea: a 3-d modeling study. J. Geophys. Res. Oceans 126 (5). https://doi.org/10.1029/2020jc016895.

Shum, C.K., Woodworth, P.L., Andersen, O.B., Egbert, G.D., Francis, O., King, C., Klosko, S.M., Le Provost, C., Li, X., Molines, J., Parke, M.E., Ray, R.D., Schlax, M.G., Stammer, D., Tierney, C.C., Vincent, P., Wunsch, C.I., 1997. Accuracy assessment of recent ocean tide models. J. Geophys. Res.: Oceans 102 (C11), 25173–25194. https://doi.org/10.1029/97JC00445.

Stammer, D., Ray, R.D., Andersen, O.B., Arbic, B.K., Bosch, W., Carrère, L., Cheng, Y., Chinn, D.S., Dushaw, B.D., Egbert, G.D., Erofeeva, S.Y., Fok, H.S., Green, J.A.M., Griffiths, S., King, M.A., Lapin, V., Lemoine, F.G., Luthcke, S.B., Lyard, F., Yi, Y., et al., 2014. Accuracy assessment of global barotropic ocean tide models. Rev. Geophys. 52 (3), 243–282. https://doi.org/10.1002/2014RG000450.

Sun, Z., Zhang, H., Xu, D., Liu, X., Ding, J., 2020. Assessment of wave power in the South China Sea based on 26-year high-resolution hindcast data. Energy 197, 117218. https://doi.org/10.1016/j.energy.2020.117218.

Taguchi, E., Stammer, D., Zahel, W., 2014. Inferring deep ocean tidal energy dissipation from the global high-resolution data-assimilative HAMTIDE model. J. Geophys. Res.: Oceans 119 (7), 4573–4592. https://doi.org/10.1002/2013JC009766.

Taylor, K.E., 2001. Summarizing multiple aspects of model performance in a single diagram. J. Geophys. Res.: Atmos. 106 (D7), 7183–7192. https://doi.org/10.1029/2000JD900719.

Tong, J.Q., Lei, F.H., Mao, Q.W., Qi, Y.Q., 2010. Barotropic tidal energy flux and tidal energy dissipation in the South China Sea without considering local induced tidal potential. J. Trop. Oceanogr. 29 (3), 1–9. https://doi.org/10.11978/j.issn.1009-5470.2010.03.001.

Wang, Z.J., Wang, Z.W., 2019. A review on tidal power utilization and operation optimization. IOP Conf. Ser.: Earth Environ. Sci. 240, 052015. https://doi.org/10.1088/1755-1315/240/5/052015.

Waters, S., Aggidis, G., 2016. Tidal range technologies and state of the art in review. Renew. Sustain. Energy Rev. 59, 514–529. https://doi.org/10.1016/j.rser.2015.12.347.

Wiatros-Motyka, M., et al., 2023. Global Electricity Review 2023 Report. Ember.

Xie, X., Liu, Q., Zhao, Z., Shang, X., Cai, S., Wang, D., Chen, D., et al., 2018. Deep sea currents driven by breaking internal tides on the continental slope. Geophys. Res. Lett. 45 (12), 6160–6166. https://doi.org/10.1029/2018gl078372.

Yanagi, T., Takao, T., Morimoto, A., 1997. Co-tidal and co-range charts in the South China Sea derived from satellite altimetry data. Lamer 35 (1997), 85–93. ⟨http://www.sfjo-lamer.org/la_mer/35-3/35-3-1.pdf⟩.

Yang, Q., Tian, J., Zhao, W., Liang, X., Zhou, L., 2014. Observations of turbulence on the shelf and slope of northern South China Sea. Deep Sea Res. Part I: Oceanogr. Res. Pap. 87, 43–52. https://doi.org/10.1016/j.dsr.2014.02.006.

Ye, A.L., Robinson, I.S., 1983. Tidal dynamics in the South China Sea. Geophys. J. Int. 72 (3), 691–707. https://doi.org/10.1111/j.1365-246X.1983.tb02827.x.

Yusoff, N.M., Ramli, N., Mohamed, M., 2015. Investigation of the potential harnessing tidal energy in Malaysia. ARPN J. Eng. Appl. Sci. 10 (21), 9835–9841.

Zahel, W., 1995. Assimilating ocean tide determined data into global tidal models. J. Mar. Syst. 6 (1), 3–13. https://doi.org/10.1016/0924-7963(94)00014-3.

Zhang, Y., Lin, Z., Liu, Q., 2014. Marine renewable energy in China: current status and perspectives. Water Sci. Eng. 7 (3), 288–305. https://doi.org/10.3882/j.issn.1674-2370.2014.03.005.

Zheng, G., Tang, D., 2007. Offshore and nearshore chlorophyll increases induced by typhoon winds and subsequent terrestrial rainwater runoff. Mar. Ecol. Prog. Ser. 333, 61–74. https://doi.org/10.3354/meps333061.

Zheng, J., Dai, P., Zhang, J., 2015. Tidal stream energy in China. Procedia Eng. 116, 880–887. https://doi.org/10.1016/j.proeng.2015.08.377.

Zhou, M., Wang, G., 2015. Responses of atmospheric circulation to sea surface temperature anomalies in the South China Sea. Ocean Sci. 11 (6), 873–878. https://doi.org/10.5194/os-11-873-2015.

Zu, T., Gan, J., Erofeeva, S.Y., 2008. Numerical study of the tide and tidal dynamics in the South China Sea. Deep Sea Res. Part I: Oceanogr. Res. Pap. 55 (2), 137–154. https://doi.org/10.1016/j.dsr.2007.10.007.